Combined Experimental and Theoretical Study of the Vibronic Spectra of Perylenecarboximides

Florian P. Diehl,[†] Claudia Roos,[†] Hans-Christian Jankowiak,[‡] Robert Berger,[‡,§] Andreas Köhn,*[,†] Gregor Diezemann,[†] and Thomas Basché[†]

Johannes Gutenberg-University, Institute of Physical Chemistry, Jakob-Welder-Weg 11, D-55099 Mainz, Germany, and Frankfurt Institute for Advanced Studies, Johann Wolfgang Goethe-University, Ruth-Moufang-Str. 1, D-60438 Frankfurt am Main, Germany

Received: October 14, 2009

Absorption and emission spectra of perylene-3,4-dicarboximide (PMI) and perylene-3,4,9,10-tetracarboxdiimide (PDI) derivatives embedded in a thin polymer film were measured by room-temperature bulk and low-temperature single-molecule spectroscopy. In contrast to bulk line narrowing spectra, the low-temperature single-molecule data allowed to unambiguously resolve the vibrational fine structure of the emission spectra. Additionally, the emission spectra were calculated by quantum chemical methods within the Franck−Condon approximation for various N-substituted derivatives of PMI and PDI. The experimental as well as calculated emission spectra are dominated by two spectral regions of high vibronic activity, a band system ranging from the 0−0 transition (at ΔE_{0-0}) down to 600 cm^{-1} below ΔE_{0-0} and a band system between approximately 1250 and 1700 cm^{-1} below ΔE_{0-0}. Apart from the wavenumber region close to ΔE_{0-0} (down to 100 cm^{-1} below ΔE_{0-0}), good agreement is found between the calculated and experimental spectra, allowing a clear-cut assignment of the dominant vibrational modes. There are, however, discrepancies in the intensities in particular for low-frequency vibrational modes. These differences between theory and experiment are tentatively attributed to linear electron−phonon coupling which is completely neglected in the calculations and hindered internal rotation that is not properly accounted for in the harmonic approximation. Furthermore, in the experimental spectra, at the bulk as well as the single-molecule level, significant differences between PMI and PDI are observed which are attributed to stronger interactions with the matrix environment in the case of PMI due to the permanent electric dipole moment of that molecule.

1. Introduction

Perylenecarboximide dyes have found widespread use as car coloration pigments[1] and as active optical components in organic light emitting diodes (OLEDs),[2,3] field-effect transistors (OFETs),[4] and solar cells.[5,6] This wide range of applications is based on their excellent photophysical properties, which comprise large absorption coefficients, high fluorescence quantum yields, and outstanding chemical, thermal, and photochemical stabilities. The photophysical properties of perylenecarboximides in the bulk have been probed by numerous techniques,[7−13] yielding reliable numbers for, e.g., oscillator strengths, fluorescence quantum yields, and lifetimes of these dyes.

Because of their favorable optical properties, perylene- and other rylenecarboximides have frequently been used in single-molecule spectroscopy. Although in the first investigation the higher homologue terrylenetetracarboxdiimide (TDI) was studied,[14] later on most investigations used perylenecarboximides and bay-substituted varieties, since they are commercially available and easy to process.[15−27] A further advantage of this class of dyes is that they exhibit sharp zero-phonon lines[28,29] at low temperature, which are a crucial prerequisite for high-resolution single-molecule spectroscopy.

In room-temperature single-molecule studies of perylene-3,4-dicarboximide (PMI) and perylene-3,4,9,10-tetracarboxdiimide (PDI), among other topics, conformational transitions and switching between a locally excited and a charge transfer state have been reported.[17−20,24,25,30,31] The latter observation[31] bears some relation to the work presented here because it appears to be a manifestation of the permanent dipole moment which exists in PMI (and not in PDI). In investigations at cryogenic temperatures, triplet kinetics and transition dipole strengths have been determined for PDI at the single-molecule level.[15,16] Furthermore, rylenecarboximides have served as donor and acceptor chromophores for electronic excitation energy transfer studies in multichromophoric compounds, both in the ensemble and on the single-molecule level.[30−35]

In a number of theoretical studies of PDI, among other properties, electronic transition energies and vibrational frequencies have been calculated. Engel et al.[36] studied the electronic transition energies of PDI, and Clark et al.[37] calculated the vibronic absorption spectrum of PDI and PDI-dimers using time-dependent density functional theory and showed the existence of two strong vibronic bands. Perylene dimers have also been considered by Velardez et al.[38] both in the gas phase and in a crystalline environment. The results have been used to analyze scattering data. The impact of substitutional effects has recently been investigated[39] with the result that the effect of side groups heavily relies on the nature of the linking atoms. On the other hand, the PMI chromophore has not received much attention

* To whom correspondence should be addressed. E-mail: andreas.koehn@uni-mainz.de.
[†] Johannes Gutenberg-University.
[‡] Johann Wolfgang Goethe-University.
[§] New address: TU Darmstadt, Clemens-Schöpf Institute for Organic Chemistry and Biochemistry, Petersenstr. 22, D-64287 Darmstadt, Germany.

10.1021/jp909862x © 2010 American Chemical Society
Published on Web 01/08/2010

SCHEME 1: Molecular Structures of the Compounds Investigated: N-Substituted Perylene-3,4-dicarboximide (PMI) and N,N′-Disubstituted Perylene-3,4,9,10-tetracarboxdiimide (PDI) Derivatives[a]

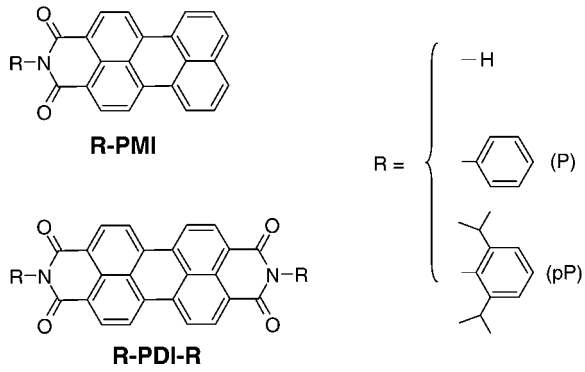

[a] R denotes the residues at the imide nitrogens. The experiments were conducted with R = pP (2,6-diisopropyl-phenyl) for PMI and PDI, respectively. The quantum chemical calculations were performed for all three residues.

in theoretical studies so far, although it was one of the constituents in several studies on larger molecular systems.[40,41]

In this contribution, we investigate perylene-3,4-dicarboximide (PMI) and perylene-3,4,9,10-tetracarboxdiimide (PDI) derivatives (Scheme 1) embedded in an amorphous host (poly(methylmethacrylate), PMMA) by means of room-temperature bulk and low-temperature single-molecule spectroscopy. Vibrationally resolved single-molecule emission spectra recorded at 1.2 K are compared to theoretical spectra calculated by quantum chemical methods for various N-substituted derivatives of PMI and PDI in a vacuum at zero temperature. On the basis of the theoretical results, most of the transitions observed in the experimental spectra can be assigned to specific vibrational modes. Besides the determination of the vibrational substructure in the emission spectra, we address the issue of coupling of the electronic transitions of PMI and PDI to the surrounding PMMA host. Significant differences between PMI and PDI are attributed to the existence of a permanent electric dipole moment in PMI which gives rise to an increased electron−phonon coupling strength and larger inhomogeneous broadening.[29,42]

2. Experimental Details

Samples for the room-temperature bulk absorption and emission spectra of pP-PMI and pP-PDI-pP in PMMA were prepared by solvent evaporation of a mixture of 3 mL of a concentrated PMMA/THF solution (200 g/L) and 300 μL of the corresponding dye/toluene solution (3×10^{-5} mol/L) on a glass coverslip. Evaporation of the solvents yielded PMMA films (thickness $\approx$ 0.3 mm) containing pP-PMI or pP-PDI-pP ($c \approx 1 \times 10^{-5}$ mol/L), respectively. Absorption spectra were measured with an Omega 20 spectrometer (Bruins Instruments) and were corrected for the solvent absorbance. Fluorescence spectra were recorded using a FluoroMax-2 fluorometer (Jobin Yvon-Spex) and were corrected for the monochromator and detector sensitivity. Although the obtained samples had good optical quality, nonuniformity of film thickness did not allow for a quantitative evaluation of the film absorption spectra. For comparison, and to determine absolute band intensities in absorption, ensemble spectra in toluene solution (10^{-6} mol/L) were measured.

Samples for the single-molecule experiments were prepared by diluting toluene solutions of pP-PMI and pP-PDI-pP (2.5×10^{-8} mol/L) with PMMA in toluene ($c = 20$ g/L) in a ratio of 1:250. Spin-coating 30 μL of these solutions on thoroughly cleaned glass cover slides at 4000 rpm for 120 s yielded thin, dye-doped polymer films (thickness $\approx$ 100 nm). The fluorescence imaging and spectroscopy of single dye molecules was conducted using a home-built variable temperature laser scanning confocal microscope that has been described in detail elsewhere.[21] For this purpose, sample and microscope objective (60×, NA = 0.85, Melles Griot) were mounted in an optical cryostat (Janis Research Company) and immersed in superfluid liquid helium ($T = 1.2$ K). An argon ion laser (Sabre Innova R DBW 15, Coherent) was used for excitation of the dye molecules at 488 nm (pP-PMI, $I = 5.2$ kW/cm^2; pP-PDI-pP, $I = 3.5$ kW/cm^2). The red-shifted fluorescence was separated by a long pass filter (pP-PMI, Semrock LP01-488RU-25; pP-PDI-pP, Omega 500 ALP) and imaged onto the entrance slit of a spectrograph (SpectraPro 500i, Acton) equipped with a liquid nitrogen cooled CCD camera (LN1100PB, 330 × 1100 pixel, Princeton Instruments). The spectrograph was run in low- (150 grooves/mm grating; 20 cm^{-1} resolution) and high-resolution mode (1800 grooves/mm grating; 2 cm^{-1} resolution). In high-resolution mode, the spectra had to be assembled from a number (up to 8) of recordings with different positions of the diffraction grating because of the finite size of the CCD chip. Potential photobleaching during spectra acquisition was checked by analyzing the corresponding fluorescence intensity trajectories. For further analysis, the spectra were corrected for the transmission curves of the corresponding long pass filters and for the sensitivity of the diffraction gratings and the CCD camera.

The low-temperature bulk emission spectrum of pP-PDI-pP in PMMA was recorded using the same setup ($\lambda_{exc} = 488$ nm, $I = 0.01$ kW/cm^2, LP500). The corresponding sample was prepared in an analogous manner to the single-molecule samples using 30 μL of a 6.5×10^{-6} mol/L solution of the dye in PMMA/toluene.

3. Computational Details

The equilibrium structures and harmonic force fields of all molecules considered in the present study were calculated using density functional theory (DFT). The electronic ground state structures were determined by applying the B3LYP hybrid functional[43] in conjunction with the polarized split valence basis set SVP.[44] Calculations concerning the first electronically excited singlet state of each molecule were performed using time dependent DFT (TDDFT) employing the same functional and basis set as for the electronic ground state. All calculations were performed with the TURBOMOLE package.[45] While analytical gradients of the electronic energy with respect to displacements of the nuclei are available for electronic ground and excited states, second derivatives were determined analytically[46] for the ground state and numerically employing finite differences of analytic gradients for the electronically excited state.

A rather tight grid (TURBOMOLE grid size 4) was used for the numerical integration of the exchange-correlation contributions. The convergence criterion for the structure optimizations was $10^{-4}\ E_h\ a_0^{-1}$ for the gradient and $10^{-6}\ E_h$ for energy changes. Numerical derivatives were done using Cartesian displacements of 0.01 a_0. The harmonic frequencies were always calculated using the mass of the most abundant isotope for the respective nucleus. Electronic transition dipole moments were calculated with TDDFT at the respective equilibrium structures.

In order to calibrate the accuracy of the above calculations, we performed additional calculations using a larger TZVP basis set[47] for selected cases. Furthermore, we used different quantum

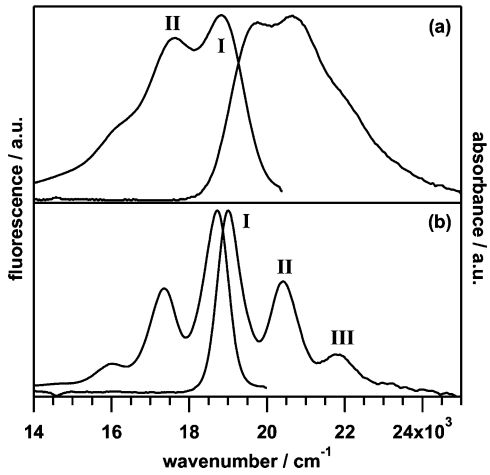

Figure 1. Absorption and emission spectra of (a) pP-PMI and (b) pP-PDI-pP in a PMMA film at room temperature.

chemical methods, namely, Møller−Plesset second-order perturbation theory (MP2) and the propagator method ADC(2)[48,49] with the SVP basis set, as also implemented in TURBOMOLE,[50] to verify the DFT results.

The vibronic emission spectra were calculated in the Franck−Condon (FC) and harmonic approximation using the program HOTFCHT.[51,52] Among other features, this program allows the calculation of vibronic spectra for molecules with up to about 200 atoms within the time-independent framework due to an efficient prescreening that drastically reduces the number of the required FC integrals. The resulting spectra reported in this work contain the FC profile which includes 99.99% of the total FC intensity. The stick representations were convoluted with Lorentzian line shapes with a full width at half-maximum (fwhm) of 2 cm^{-1}. For direct comparison with experimental emission spectra (photons per time and frequency interval), the FC profiles were multiplied by a $\tilde{\nu}^3$-dependent scaling factor, where $\tilde{\nu}$ is the emission wavenumber.

4. Results and Discussion

4.1. Experimental Absorption and Emission Spectra. ***4.1.1. Bulk Spectra.*** In Figure 1, the bulk absorption and fluorescence emission spectra of pP-PMI and pP-PDI-pP in PMMA at room temperature are displayed. As seen immediately, the overall appearances of the spectra differ strongly. The pP-PDI-pP absorption (emission) spectra are clearly dominated by the lowest (highest) energy vibronic feature. In the case of pP-PMI, the higher (lower) energy vibronic transitions are much more pronounced which, in addition to a stronger inhomogeneous broadening of these transitions (see below), gives rise to less resolved bulk spectra. In addition, the relative intensities of the higher (lower) energy vibronic transitions of pP-PMI differ in absorption and emission. Accordingly, while the bulk absorption and emission spectra of pP-PDI-pP exhibit nearly perfect mirror symmetry, the latter is clearly reduced for pP-PMI. In the former case, the energy at the intersection of the emission and absorption spectra can be interpreted as the adiabatic transition energy, ΔE_{adiab}, or the energy of the 0−0 transition, ΔE_{0-0}.[29,53] Note that this interpretation is not possible for pP-PMI, as will be discussed in section 4.1.2. The Stokes shift as determined by the energy difference between the energetically lowest absorption maximum and the highest emission maximum is more than 3 times larger for pP-PMI (925 cm^{-1}) as compared to pP-PDI-pP (285 cm^{-1}), suggesting some pronounced differences in the interaction with the polymer host.

TABLE 1: Spectroscopic Quantities of pP-PMI and pP-PDI-pP Extracted from the Bulk Spectra in PMMA and Toluene Solution, Respectively

	pP-PMI		pP-PDI-pP	
optical property	absorbance	emission	absorbance	emission
$\tilde{\nu}_{max}$/cm^{-1}	19760	18835	19010	18725
(I,II) separation[a]/cm^{-1}	900	1200	1400	1370
(I,III) separation[a]/cm^{-1}			2770	2710
Stokes shift/cm^{-1}	925		285	
intersection point/cm^{-1}	19270		18865	
ε_A^{max} [b]/(L/(mol cm))	31000		71500	
$\|\mathbf{d}\|_{abs}$[c]/D	8.1		9.0	

[a] Spectral separation of partially resolved vibronic bands denoted I, II, and III. [b] From a toluene solution. [c] From a toluene solution, corrected for the refractive index.[54]

Because of the clear separation between the S_0-S_1 and higher energy transitions, the absorption spectra allow for a quantitative determination of the oscillator strengths and absorption transition dipole moments $|\mathbf{d}|_{abs}$, respectively.[29,54] Since the nonuniform thickness of PMMA films, however, did not permit a reliable determination of extinction coefficients ε_A, the latter were extracted from the solution absorption spectra in toluene[35,55] which showed nearly no differences with respect to transition energies and relative band intensities compared to the PMMA film spectra. Whereas the obtained $|\mathbf{d}|_{abs}$ differs just by 10%, the resulting ε_A^{max} is more than twice as large for pP-PDI-pP as for pP-PMI due to stronger inhomogeneous broadening and coupling to vibrations in the latter compound. The spectroscopic quantities determined from bulk emission and absorption spectra are collected in Table 1.

4.1.2. Single-Molecule Emission Spectra. Although a number of spectral parameters can be extracted from the room-temperature bulk absorption and emission spectra shown in Figure 1 (Table 1), their information content is clearly limited. By cooling down the samples to very low temperature ($T < 10$ K), the situation does not improve in principle, because the spectra of chromophores in an amorphous host (here PMMA) are strongly inhomogeneously broadened. Accordingly, conventional bulk absorption and emission spectra of pP-PMI and pP-PDI-pP would look quite similar to the ones shown in Figure 1. By selecting a subensemble of chromophores via narrow-band laser excitation, a substantial line narrowing can be achieved in the emission spectra in the limit of weak linear electron−phonon coupling. Nevertheless, inhomogeneous contributions typically are only partly removed, because in this kind of bulk line-narrowing experiment different transitions in absorption and emission are probed.[29] In the following, we compare a bulk and a single-molecule pP-PDI-pP emission spectrum both obtained at $T = 1.2$ K with an excitation wavelength of 488 nm, i.e., narrow band laser excitation into the second vibronic transition (II) (cf. Figure 1).

As is clearly seen in Figure 2a, the gain in spectral resolution as compared to the room-temperature bulk emission spectrum (Figure 1b) is limited, although some narrow features are discernible in the bulk spectrum. In contrast, the single-molecule emission spectrum shown in Figure 2b appears as a sequence of sharp zero-phonon lines (ZPLs), because such single-molecule spectra do not suffer from pronounced inhomogeneous contributions. We want to emphasize that, in the limit of weak electron−phonon coupling (and with moderate extent of spectral diffusion), vibrationally resolved emission spectra of dye molecules dispersed in an amorphous polymer film can be routinely obtained by single-molecule spectroscopy.

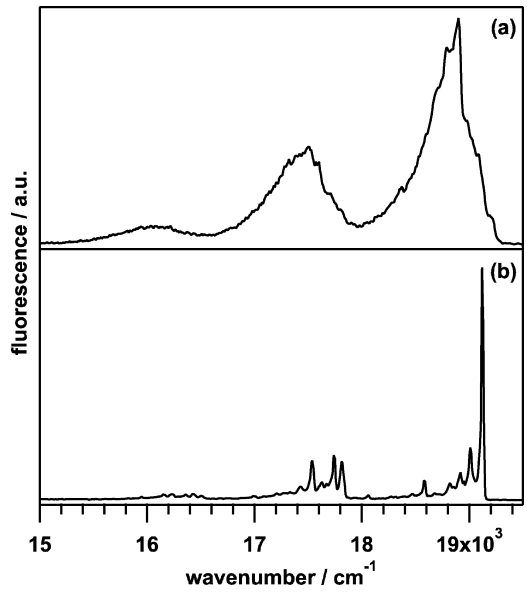

Figure 2. Bulk (a) and single-molecule (b) emission spectrum of pP-PDI-pP in PMMA at $T = 1.2$ K obtained with narrow band laser excitation of 488 nm.

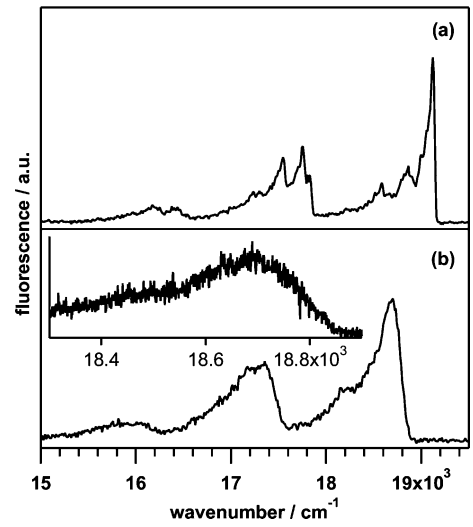

Figure 3. Typical single-molecule fluorescence emission spectra of pP-PMI in PMMA at $T = 1.2$ K. In contrast to pP-PDI-pP (Figure 2b), pP-PMI molecules show much stronger variations with respect to their spectral appearance. The corresponding limits are shown in parts a and b. The inset in part b shows the first part of the high-resolution spectrum within the region of the emission maximum.

Low-temperature single-molecule emission spectra of pP-PDI-pP and pP-PMI were recorded in low- and high-resolution mode of the spectrograph. The recording of high-resolution spectra, however, is very time-consuming and only possible for extraordinary stable molecules. Therefore, the comparison of different types of spectra in the following was based on the low-resolution mode spectra. In total, 113 pP-PDI-pP molecules embedded in thin PMMA films were investigated. A typical low-resolution mode emission spectrum is presented in Figure 2b. For more than 90% of the pP-PDI-pP molecules investigated, the spectra were unambiguously dominated by the ZPL of the purely electronic $S_0 \leftarrow S_1$ transition in both low- and high-resolution mode and the overall spectral appearance was similar to the one shown in Figure 2b. In contrast to pP-PDI-pP, pP-PMI single-molecule emission spectra (116 molecules studied) did show strong variations in their spectral appearance. For 40% of the investigated chromophores, the spectral shape was close to the one shown in Figure 3a. In these cases, clearly discernible ZPLs were observed in high-resolution mode. On the other hand, 15% of the pP-PMI molecules were characterized by a very broad emission that even in high-resolution mode did not show any indication for ZPLs (Figure 3b). In comparison to the former ones, their positions of maximum intensity are shifted on average by more than 300 cm^{-1} to lower energies. The remaining 45% of the pP-PMI molecules have been intermediate cases which typically could not be assigned unambiguously to one of the two limiting cases as represented in Figure 3a and b.

High-resolution spectra of pP-PDI-pP and pP-PMI molecules exhibiting narrow zero-phonon features and covering most of the range of vibronic activity are shown in Figure 4. Small scale spectral diffusion was found frequently for pP-PDI-pP as well as pP-PMI but is of no further importance in the present context.[56] The vibrational frequencies of the most prominent transitions are collected in Table 5 below. A detailed analysis and discussion of the vibrational structure of the spectra will be given in section 4.3 together with the results from the quantum chemical calculations. Remarkably, in contrast to the room-temperature bulk spectra (Figure 1), the single-molecule spectra of pP-PDI-pP and pP-PMI at first glance look surprisingly similar. The most prominent differences are found in the

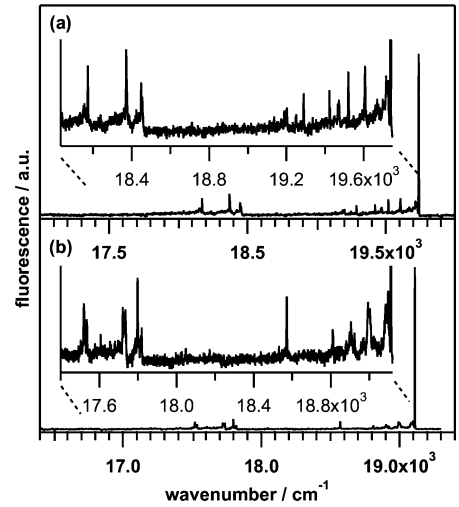

Figure 4. High-resolution emission spectra of single pP-PMI (a) and pP-PDI-pP (b) molecules. The insets show the vibrational transitions on an enlarged scale.

first vibronic band system (all vibronic transitions in a wavenumber range from 0 to 600 cm^{-1} near the 0−0 transition), while the spectroscopic features in the second vibronic band system (range from 1250 to 1700 cm^{-1}) are roughly the same (apart from the doubling of the lines in case of PDI, cf. section 4.3).

For further comparison of the pP-PMI and pP-PDI-pP single-molecule spectra, we determined the intensity ratio between the purely electronic ZPL (the ZPL of the 0−0 transition) and the full $S_0 \leftarrow S_1$ transition (up to 4000 cm^{-1} below the 0−0 transition), denoted as I_{ZPL}/I_{total}. This quantity is a measure for the coupling of the electronic transition to the vibrational modes, including both intramolecular vibrations and vibrations of the matrix environment (phonons). A separation of these two contributions is difficult; an estimate of the so-called Debye−Waller factor[28,29,57] will be discussed at the end of this paragraph. To determine the ratio I_{ZPL}/I_{total}, a Gaussian is fitted to the high-energy tail of the ZPL and subsequent integration over its full spectral range gives I_{ZPL}. Division by the integrated intensity

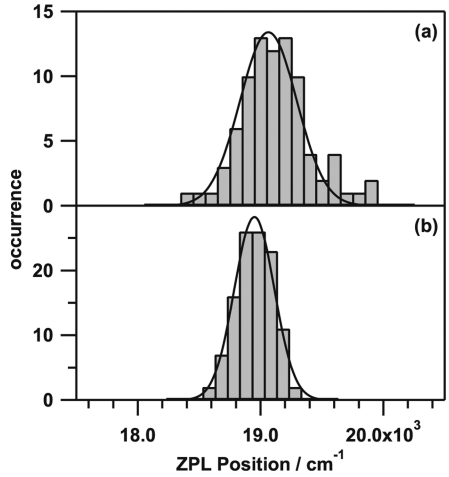

Figure 5. ZPL distributions of (a) pP-PMI and (b) pP-PDI-pP in PMMA at $T = 1.2$ K with Gaussians fitted to the data.

of the full $S_0 \leftarrow S_1$ transition I_{total} yields the desired quantity. The choice of a Gaussian is justified, since the line shape of the ZPL is given by the instrumental band-pass which is well represented by a Gaussian. For the analysis, only emission spectra of molecules showing a clearly resolved ZPL in the low-resolution mode (Figure 2b and Figure 3a) were considered. The probability density distribution of I_{ZPL}/I_{total} for pP-PMI exhibits a peak at 7.7%, whereas the corresponding distribution for pP-PDI-pP shows a maximum around 16.5%. These results indicate that the pP-PMI electronic transition features a stronger coupling to phonons and intramolecular vibrations. In order to get an estimate of the relative weight of the two contributions, we determined the Debye−Waller factor, which is directly connected to the linear electron−phonon coupling strength.[28,29,57] For the purely electronic 0−0 transition, it can be obtained as $\alpha_D = (I_{ZPL})/(I_{ZPL} + I_{PSB})$. Since the phonon sideband (PSB) could not be completely separated from low-frequency intramolecular vibrations, the integration over the PSB was limited to 100 cm^{-1} and the corresponding average values of the Debye−Waller factors (pP-PMI, $\alpha_D = 0.15$; pP-PDI-pP, $\alpha_D = 0.4$) can only be considered as approximate. Nevertheless, they appear reliable enough to indicate a stronger electron−phonon coupling for pP-PMI.

In Figure 5, the distributions of the purely electronic ZPL positions for pP-PMI and pP-PDI-pP in PMMA are plotted. It is found that the distribution width for pP-PMI in PMMA (fwhm: 555 cm^{-1}) equals 1.5 times the value of pP-PDI-pP in PMMA (fwhm: 380 cm^{-1}), indicating a stronger inhomogeneous broadening for pP-PMI. In addition, the maximum of the inhomogeneous distribution of pP-PDI-pP (18950 cm^{-1}) agrees, within the accuracy of measurement and fitting procedure, with the intersection point of absorption and emission (ΔE_{adiab}) determined from the bulk spectra (Table 1). In the case of pP-PMI, the maximum of the ZPL distribution (at 19090 cm^{-1}) is shifted by about 180 cm^{-1} to lower energies when compared to the intersection point of the absorption and emission spectrum. This is consistent with the fact that the intersection points of molecules exhibiting no mirror symmetry in normalized bulk absorption and emission slightly overestimate the center positions of the corresponding electronic 0−0 transitions by ca. 1%.[53] Before we discuss the experimental findings further, in the next section, we present the results of quantum chemical calculations on differently substituted PMI and PDI derivatives.

4.2. Results of Theoretical Study. ***4.2.1. Transition Energies, Dipole Moments, and Charge Distributions of PMI and PDI.*** Quantum chemical calculations allow us to gain insight into the electronic and structural changes upon $S_1 \leftarrow S_0$ excitation. They also enable us to investigate the influence of the residues attached to the imide nitrogens on the chromophores of PMI and PDI. Apart from the 2,6-diisopropyl-phenyl group (pP), which is the residue of the compounds used in the experiments, we study hydrogen- (H) and phenyl-substituted (P) PMI and PDI, to be denoted as R-PMI and R-PDI-R, R = H, P, pP, in the following (see Scheme 1).

The calculated transition energies and electronic transition dipole moments are listed in Table 2. Here, ΔE_{em} denotes the vertical energy separation between the minimum of the excited state Born−Oppenheimer (BO) surface ($E_{min}(S_1)$) and the ground state BO surface. Analogously, ΔE_{abs} is the vertical energy difference between the minimum of the ground state BO surface and the excited state BO surface. These values often are used as estimates for the band maxima of the absorption and emission spectra (due to the Franck−Condon principle). However, as the vibronic spectra of the perylenecarboximides are dominated by the 0−0 transition, these numbers are not well suited for that purpose. It is better to use the adiabatic excitation energy $\Delta E_{adiab} = E_{min}(S_1) - E_{min}(S_0)$ as an approximation for the absorption maximum. Note that for harmonic BO surfaces with equal vibrational frequencies ΔE_{adiab} coincides with $\Delta E_{0-0} = E_{\nu=0}(S_1) - E_{\nu=0}(S_0)$, the energy difference including the zero-point vibrational contribution.

Our calculations show that the different residues bound to the imide nitrogen have only a minor influence on the transition energies. Those vary by 800 cm^{-1} at most for the three residues examined. The ΔE_{0-0} values obtained for the pP-substituted chromophores predict purely electronic ZPL positions at about 20.1×10^3 cm^{-1} for PMI and at 18.3×10^3 cm^{-1} for PDI. The larger values for the transition energies in the case of PMI as compared to PDI can qualitatively be understood in terms of the larger HOMO−LUMO gap for PMI due to the smaller extension of the π-system.

Our results in Table 2 indicate a sizable effect of the phenyl residues on the electronic transition dipole moments. These increase by about 0.5 to 0.6 D for PMI and 1.1 to 1.2 D for PDI upon replacing the hydrogen atom by phenyl groups. As suggested previously,[34] this effect can be understood as resulting from the polarizability of the π-systems of the phenyl moieties giving rise to an off-resonant contribution to the transition moments. Generally, the calculated electronic transition dipole moments for PMI are smaller than for PDI by about 1.0 to 1.5 D. We note that the small difference between the electronic transition dipole moments at the ground and excited state minima, $|\mathbf{d}|_{abs}$ and $|\mathbf{d}|_{em}$, indicates a very weak dependence on the nuclear coordinates and thus supports the application of the Condon approximation in simulating the vibronic spectra, cf. section 4.2.2.

Insight into the nature of the excited states is gained from the plots of the difference density between ground and excited state, which are shown in Figure 6 for the hydrogen substituted species of PMI and PDI. Inclusion of different residues at the imide nitrogen leads only to negligible changes in the difference densities. The plots indicate that nearly all changes in the electron density take place in the π-system. We find an alternation of electron density increase and decrease on the lateral C−C bonds along the main axis, whereas the density in the center of the molecule remains nearly unchanged. The pattern is very similar for both PMI and PDI, although for the

TABLE 2: Calculated (B3LYP/SVP) Vertical Electronic Transition Energies ΔE_{abs} and ΔE_{em} with Transition Dipole Moments $|\mathbf{d}|_{abs}$ and $|\mathbf{d}|_{em}$ as Well as the 0−0 and Adiabatic Transition Energies ΔE_{0-0} and ΔE_{adiab} of PMI and PDI with Different Residues Bound to the Imide Nitrogen Atom[a]

molecule	Ex. state symmetry	$\Delta E_{abs}/(hc\ 10^3\ cm^{-1})$	$\|\mathbf{d}\|_{abs}$/D	$\Delta E_{em}/(hc\ 10^3\ cm^{-1})$	$\|\mathbf{d}\|_{em}$/D	$\Delta E_{0-0}/(hc\ 10^3\ cm^{-1})$	$\Delta E_{adiab}/(hc\ 10^3\ cm^{-1})$
H-PMI	$^1A_1$	20.9	7.07	19.0	7.32	20.3	20.0
H-PDI-H	$^1B_{1u}$	19.6	8.13	17.8	8.41	19.1	18.7
P-PMI	^1A	20.8	7.61	18.9	7.88	20.0	19.9
P-PDI-Ph	$^1B_1$	19.5	9.25	17.6	9.58	18.4	18.5
pP-PMI	^1A	20.7	7.77	18.8	8.04	20.1	19.8
pP-PDI-pP	$^1B_1$	19.3	9.32	17.4	9.61	18.3	18.3

[a] The point groups of the equilibrium structures are as follows: H-PMI, C_{2v}; P-PMI, C_2; pP-PMI, C_2; H-PDI-H, D_{2h}; P-PDI-P, D_2; pP-PDI-pP, D_2. All molecules are oriented such that the long molecular axes coincide with the z-axis.

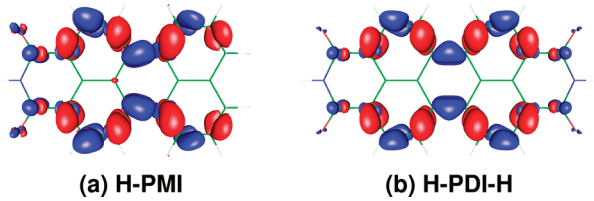

Figure 6. Isosurfaces (0.001 a_0^{-3}) of the calculated electron density differences $\Delta\rho = \rho(S_1) - \rho(S_0)$ between the first electronically excited state (S_1) and the electronic ground state (S_0) for H-PMI and H-PDI-H at the B3LYP/SVP level. Areas of electron density enhanced upon excitation are colored in blue and those of lowered electron density in red.

TABLE 3: Permanent Electric Dipole Moments of PMI with Different Residues at the Imide Nitrogen Atom, as Calculated at the B3LYP/SVP Level[a]

molecule	μ_g	μ_e	$\Delta\mu$
H-PMI	6.45	7.36	0.91
P-PMI	5.69	6.69	1.00
pP-PMI	6.29	7.23	0.94

[a] The symbols μ_g and μ_e denote the ground state (S_0) and excited state (S_1) electric dipole moments, and the difference $\Delta\mu = \mu_e - \mu_g$. All values in debye.

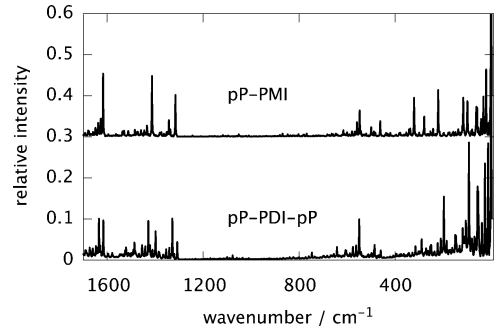

Figure 7. Emission spectrum of pP-PMI (top) and pP-PDI-pP (bottom), calculated at the B3LYP/SVP level. The abscissa corresponds to the negative increment to the 0−0 transition, the emission intensity is given in relative units (the 0−0 emission peak has been scaled to 1), and the baseline of pP-PMI was shifted up by 0.3 units.

former a slight distortion is observed due to the lack of a center of symmetry. A Löwdin population analysis indicates that in the case of PMI the increase of charge density on the imide group is roughly twice as large as in the case of PDI, where two imide groups "compete" for the extra charge. This change of the partial charge on the imide group results in a change of the permanent electric dipole moment $\Delta\mu = \mu_e - \mu_g$ for PMI; see Table 3. Whereas the resulting absolute ground and excited state electric dipole moments are somewhat dependent on the considered residues, the difference between those is almost unaltered and amounts to $\Delta\mu = 0.9$ to 1.0 D. We mention that PDI has a center of symmetry and therefore no permanent electric dipole moment.

The changes in electron density are related to changes of the molecular equilibrium structures induced upon electronic excitation. Regions of increased electron density in Figure 6 indicate an increasing double bond character of the corresponding C−C bonds and decreased density a decreasing double bond character. The changes in bond lengths are characterized by a shortening of C−C bonds directed along the molecular main axis and an elongation of most of the C−C bonds along the short molecular axis lying in the molecular plane. The calculated magnitudes of bond length changes between electronic ground and excited state amount to up to 3.1 pm in H-PMI and 2.8 pm in H-PDI-H at the B3LYP/SVP level. These results are in good agreement with those of calculations at the B3LYP/TZVP level that can be found in the Supporting Information. Similar calculations performed at the MP2/SVP and ADC(2)/SVP level show the same trends, cf. the Supporting Information.

4.2.2. Vibronic Emission Spectra. The vibronic emission spectra were calculated for isolated R-PMI and R-PDI-R molecules using the residues H, P, and pP at the imide nitrogens, as introduced in the preceding section and Scheme 1. Only the vibrational ground state of the initial electronic state is assumed to be populated, which closely resembles the experimental situation at low temperatures. In order to compare the spectra, all 0−0 transition intensities were normalized to unity. The spectra of both pP-PMI and pP-PDI-pP (Figure 7) are composed mainly of two groups of vibronic transitions. The first one ranges from 0 to about 600 cm^{-1} below ΔE_{0-0}, and the second one shows up in a wavenumber range from about 1250 to 1700 cm^{-1} below ΔE_{0-0}. In the following, we will discuss the two band regions separately starting with PMI.

We note that the neglect of anharmonic effects leads to errors in the wavenumbers up to roughly 100 cm^{-1} and might particularly for low-wavenumber modes give rise to different mode-mixing. Nevertheless, some interesting features can be extracted from the calculations. The first vibronic bands (0 to 600 cm^{-1} below the 0−0-transition wavenumber) for the PMI and PDI derivatives are displayed in Figure 8. One important finding is that with the exception of H-PMI and H-PDI-H quite a number of normal modes with nonvanishing FC factors exist in the wavenumber region down to 100 cm^{-1} below ΔE_{0-0}, some of them involving even multiple excitations of nontotally symmetric modes. It is apparent from Figure 8 that the residues have a large impact on the spectra in this frequency regime.

The most prominent transition wavenumbers for PMI (with corresponding wavenumbers smaller than $\Delta E_{0-0}/(hc)$ − 100 cm^{-1}) are listed in Table 4. The dominant transition labeled "a" at 279 cm^{-1} for H-PMI corresponds to a breathing mode.

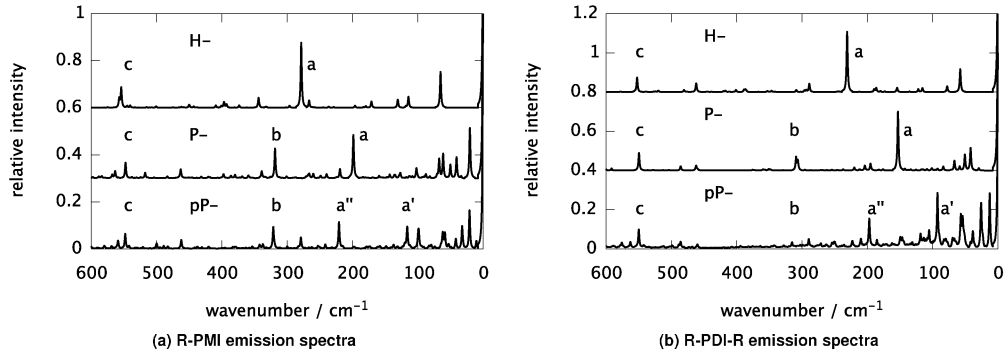

Figure 8. First vibronic band region (0 to 600 cm^{-1} below ΔE_{0-0}) of the emission spectra for R-PMI and R-PDI-R with R = H, P, and pP (from top to bottom) calculated at the B3LYP/SVP level. Note that the baselines of the former two are shifted and that the wavenumber corresponds to the negative of the increment to the 0−0 transition wavenumber.

TABLE 4: Harmonic Vibrational Wavenumbers of R-PMI, with R = H, P, or pP Bound to the Imide Group, Calculated at the B3LYP/SVP Level

harmonic vibrational wavenumbers $\tilde{\omega}$ in cm^{-1}					
H-PMI		P-PMI		pP-PMI	
$\tilde{\omega}$	label	$\tilde{\omega}$	label	$\tilde{\omega}$	label
279	a	199	a	116	a′
				221	a″
		319	b	321	b
554	c	548	c	548	c
1315	d	1317	d	1316	d
1414	e	1414	e	1414	e
1617	f	1618	f	1617	f

In contrast to the H-PMI spectrum, an additional mode "b" occurs for P-PMI and pP-PMI. The origin of this mode can be understood as a splitting of mode a in the H-PMI spectrum. The two resulting modes are best characterized as in-phase and out-of-phase linear combinations of a breathing mode of the PMI skeleton and a "translational" mode of the phenyl residue. Going from P-PMI to pP-PMI, we find that breathing mode "a" splits into two modes "a′" (at 116 cm^{-1}) and "a″" (at 221 cm^{-1}). For both modes, there is a large contribution from vibrations of the pP moieties (rocking modes) with different phases. At lower vibronic emission frequencies, the spectra of differently substituted PMI hardly show any dependence on the chosen residue. For example, the mode denoted by "c", a breathing mode along the short molecular axis, occurs at about 550 cm^{-1} in all three spectra, cf. the Supporting Information.

The spectra of the various PDI derivates show very similar features as the corresponding PMI spectra, cf. Figure 8. The main difference is the shift of the modes "a" and "b" to somewhat lower harmonic wavenumbers due to the larger reduced mass of PDI. The corresponding transition wavenumbers and normal modes are displayed in the Supporting Information.

The results for the second vibronic band region (1250 to 1700 cm^{-1} below ΔE_{0-0}) are shown in Figure 9a for PMI and in Figure 9b for PDI. It is obvious from Figure 9a that there are three transitions in the case of PMI, labeled "d", "e", and "f", and six for PDI, cf. Figure 9b, with harmonic vibrational wavenumbers almost independent of the residues bonded to the imide group. As indicated by the notation in Table 4 (and similarly in the supplement for PDI), each of the three most intense modes of PMI appears as a doublet of modes for PDI. All of these modes mainly involve the chromophore backbones, and their wavenumbers are almost independent of the residues bound to the imide groups, cf. Figures B5 and C7 of the Supporting Information. The doublets in the PDI spectra can be attributed to different linear combinations (in-phase and out-of-phase) of skeleton vibrations that are highly symmetric with respect to the center of symmetry. For PMI, the symmetry is broken, and only one combination leads to a significantly strong FC factor.

4.3. Comparison between Experiment and Theory. The calculated wavenumbers for the purely electronic transitions of pP-PMI (20.1×10^3 cm^{-1}) and pP-PDI-pP (18.3×10^3 cm^{-1}) compare satisfactorily with the experimental averages for emission in a PMMA matrix (pP-PMI, 19.1×10^3 cm^{-1}; pP-PDI-pP, 18.95×10^3 cm^{-1}). Also, the theoretical values for the absorption electronic transition dipole moments (pP-PMI, 7.8 D; pP-PDI-pP, 9.3 D) are in reasonable agreement with the experimentally obtained values for pP-PMI (8.1 D) and pP-PDI-pP (9.0 D) in a toluene solution (corrected with the refractive index[54]), cf. Tables 1 and 2.

In Table 5, we present the experimentally determined fundamental vibrational wavenumbers for selected transitions of large intensity and compare them to the corresponding theoretical (harmonic) values. There is overall good agreement for both, pP-PMI and pP-PDI-pP, the maximum deviations in vibrational wavenumbers being on the order of 50 cm^{-1}. From a direct comparison of the experimental and theoretical spectra, presented in Figure 10, one can see that the assignment of most of the intensive lines is straightforward. In the wavenumber range down to 100 cm^{-1} below ΔE_{0-0}, however, the intensities are grossly overestimated in the calculations. The reason for this behavior can qualitatively be understood when recognizing that in this wavenumber range many of the vibrations of the pP residues are found, in particular for PDI, cf. Figure 8. These low-frequency vibrations are likely to be frozen in a solid matrix. Furthermore, the description of the methyl group dynamics in terms of harmonic vibrations is known to give qualitatively wrong results in low-temperature solids, where usually rotational tunneling of these groups is observed.[58] Within the second vibronic band, the assignment of calculated transitions to the experimental data does not pose any problem, leaving aside that each peak is again accompanied by transitions involving excitations of the above-mentioned low-frequency modes.

Concerning transition intensities, a more quantitative comparison is achieved when the calculated ratios I_{ZPL}/I_{total} are contrasted with the values determined experimentally. These ratios differ strongly from the theoretically predicted values for pP-PMI (theory, 16.3%; exp., 7.7%) and pP-PDI-pP (theory, 8.0%; exp., 16.5%), cf. Table 6. As already discussed above, many of the vibrations of the isopropyl groups are expected to be frozen in a solid matrix. Thus, it makes sense to compare

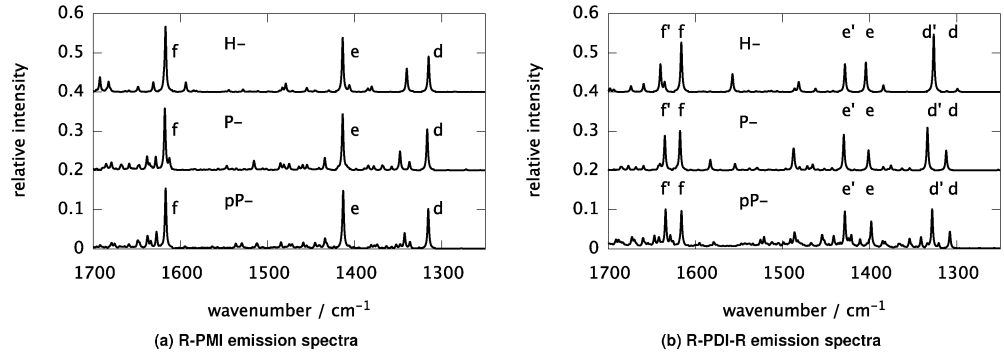

Figure 9. Second vibronic band region (1250 to 1700 cm^{-1} below ΔE_{0-0}) of the emission spectra for R-PMI and R-PDI-R with R = H, P, and pP (from top to bottom) calculated at the B3LYP/SVP level. Note that the baselines of the former two are shifted and that the wavenumber corresponds to the negative of the increment to the 0−0 transition wavenumber.

TABLE 5: Characteristic Fundamental Vibrational Wavenumbers in the Experiment and Corresponding Harmonic Vibrational Wavenumbers in the Calculation for pP-PMI and pP-PDI-pP at the B3LYP/SVP Level

vibrational wavenumbers in cm^{-1}					
pP-PMI			pP-PDI-pP		
Exp.	Calc.	label	Exp.	Calc.	label
			118	93	
131	116				
218	221	a	207	197	a
266	279				
316	321	b	301	315	b
449	462				
535	548	c	540	550	c
1290	1316	d	1291	1308	d
			1312	1328	d′
1368	1414	e	1375	1389	e
			1389	1429	e′
1566	1617	f	1577	1616	f
			1591	1634	f′

the experimentally determined ratios to those calculated using phenyl residues, which are given by 17.8% for P-PMI and by 24.7% for P-PDI-P. These values are not in quantitative agreement with the experimental ones, but they reproduce the finding that the value for pP-PMI is smaller than the one for pP-PDI-pP. Keeping in mind that the calculations did not take care of couplings to phonons in the matrix environment, the remaining discrepancy can be rationalized as follows.

A crucial difference between PMI and PDI is the lack of a center of symmetry for PMI giving rise to a permanent electric dipole moment, which in turn will affect the spectroscopic behavior of the PMI chromophore in a host matrix. We note that the low symmetry of insertion sites in the amorphous PMMA matrix most likely will also induce permanent electric dipole moments in the centrosymmetric PDI chromophore. Induced electric dipole moments, however, will affect both chromophores and are not thought to be the main origin for the significant differences of pP-PMI and pP-PDI-pP as reported here. Accordingly, we conclude that in the case of pP-PMI due to the permanent electric dipole moment the coupling of its first electronic transition to the environment is stronger than for pP-PDI-pP. Along these lines, the quantum chemical calculations in section 4.2.1 had shown that the change of the partial charge on the imide group in the case of PMI leads to a dipole moment difference between the ground and excited state. From former spectral hole-burning experiments, it is well-known that the linear electron−phonon coupling strength scales with the dipole moment changes $\Delta\mu$ upon electronic excitation.[42] As already discussed in section 4.1.2, the Debye−Waller factor of pP-PMI ($\alpha_D = 0.15$) is considerably smaller than the one of pP-PDI-pP ($\alpha_D = 0.4$), which is a clear-cut indication of a stronger electron−phonon coupling in the former case. Hence, we assume that a main reason for the differences between experimental and theoretical (residue: P) intensity ratios I_{ZPL}/I_{total} is the coupling of the electronic transitions to the host phonons, a contribution which is not accounted for in the theoretical treatment. This particular coupling is assumed to lower the intensities of the ZPLs and to lead to an increased difference between the ratios of PMI and PDI (see lines 2 (P) and 4 (pP(exp.)) in Table 6).

Besides the stronger linear electron−phonon coupling, also the larger Stokes shift (Figure 1) and inhomogeneous broadening (Figure 5) of pP-PMI as compared to pP-PDI-pP can be interpreted as signatures of the permanent electric dipole moment in PMI. Of particular interest is the appearance (15%) of broad unstructured and red-shifted single-molecule emission spectra in the case of pP-PMI (Figure 3b) which have not been found for pP-PDI-pP. Similar observations have been reported for room-temperature single-molecule studies of pP-PMI linked to a pentaphenyl bisfluorene.[24] In that case, the broad unstructured spectra were more strongly red-shifted and attributed to emission from a charge transfer state thought to exist in the more polar environments offered by the heterogeneous PMMA matrix. The "normal" more structured spectra were assigned to emission from the locally excited state. Considering the pP-PMI studied here, the following scenario is conceivable. The permanent electric dipole moment of pP-PMI may slightly favor (as compared to pP-PDI-pP) the insertion of the molecules into the more polar environments of the PMMA host. Upon electronic excitation, the partial charge on the imide group of pP-PMI may be enhanced for molecules residing in these polar environments, giving rise to some charge transfer character of the optical transition. This in turn will lead to a significant increase of the linear electron−phonon coupling strength and a concomitant disappearance of the zero-phonon line. As a result, broad unstructured spectra are obtained.

5. Conclusions

We investigated two perylenecarboximide dyes (pP-PMI, pP-PDI-pP) embedded in an amorphous host by means of room-temperature bulk and low-temperature single-molecule spectroscopy. Experimentally, we observed different spectral shapes of the bulk absorption and emission as well as the single-molecule emission spectra. By performing measurements with high spectral resolution, we were able to resolve the vibrational fine structure of the single-molecule emission spectra. In order to analyze the experimental findings, we performed quantum

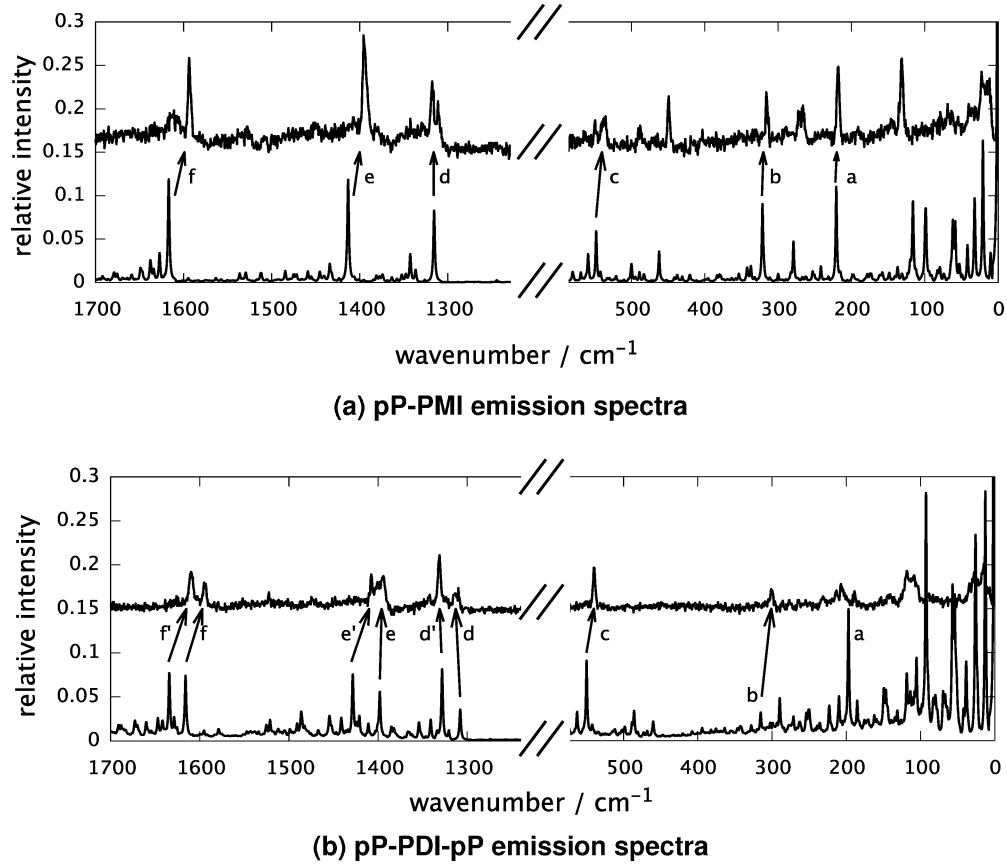

Figure 10. Emission spectra measured by single-molecule spectroscopy (shifted baseline, the same high-resolution spectra as shown in Figure 4) and calculated for pP-PMI (a) and pP-PDI-pP (b) at the B3LYP/SVP level (bottom).

TABLE 6: Calculated Intensity Ratio I_{ZPL}/I_{total} for R-PMI and R-PDI-R, R = H, Phenyl (P), and Diisopropyl-phenyl (pP), Determined at the B3LYP/SVP Level

	(I_{ZPL}/I_{total})/%	
residue	R-PMI	R-PDI-R
H	25.7	27.5
P	17.8	24.7
pP	16.3	8.0
pP(exp.)	7.7	16.5

chemical calculations of a number of spectroscopically accessible quantities including transition energies, electric dipole moments, electronic transition dipole moments, and vibronic emission spectra for differently substituted R-PMI and R-PDI-R with R = H, phenyl, and 2,6-diisopropyl-phenyl. The electronic transition dipole moments in all cases were very similar for absorption and emission, which is taken as a hint for the applicability of the Condon approximation in the calculation of the spectra. The computed vibronic emission spectra of all compounds investigated showed two clearly separated vibronic band regions. Excellent agreement between calculated and experimentally determined vibrational wavenumbers was found with the maximum deviation being on the order of 50 cm^{-1}. This allows us to assign most of the relevant transitions observed experimentally apart from the wavenumber region close to the 0−0 transition (down to about 100 cm^{-1} below ΔE_{0-0}). In the first vibronic band system (down to roughly 600 cm^{-1} below the 0−0-transition wavenumber), mostly breathing modes of the molecules give rise to the prominent lines, while in the second vibronic band system (1250 to 1700 cm^{-1} below ΔE_{0-0}) mainly backbone vibrations are important. The influence of the different residues R can safely be neglected in this second vibronic band system. Considering the wavenumber region down to 100 cm^{-1} with respect to the 0−0-transition wavenumber, however, the phenyl residues (P, pP) give rise to a number of transitions the origins and intensities of which are not fully understood at present. The intensity differences between experimental and theoretical spectra lines in this wavenumber region are additionally attributed to linear electron−phonon coupling which was not taken into account in the calculations. Comparing the experimental results of pP-PMI and pP-PDI-pP, there appears evidence that the permanent electric dipole moment in pP-PMI leads to a stronger coupling to the PMMA host. Besides an increase in electron−phonon coupling strength, larger inhomogeneous broadening and occasionally very broad unstructured single-molecule spectra have been observed for pP-PMI. In future experimental work, it will be interesting to apply electric fields[59] in combination with single-molecule excitation spectroscopy of pP-PMI and pP-PDI-pP to compare the magnitude of the linear contribution to the Stark shift and get more insight into local fields and symmetry breaking by the environment. Both from the theoretical and experimental side, it would be desirable to arrive at an improved understanding of the origin of low-frequency vibronic modes. Such modes may assist electronic excitation energy transfer in donor−acceptor dyads,[60] where the donor and acceptor moieties are linked by phenylene bridges.[33]

Acknowledgment. We thank Jürgen Gauss and Gerald Hinze for stimulating discussions and Klaus Müllen for providing the perylene dyes investigated in this study. This work was supported by the Deutsche Forschungsgemeinschaft via the Sonderforschungsbereich (SFB) 625. R.B. acknowledges financial support from the Volkswagen foundation.

Supporting Information Available: Figures and tables with calculated bond length changes of H-PMI and H-PDI-H upon excitation. Visualizations of important normal modes of R-PMI and R-PDI-R. This material is available free of charge via the Internet at http://pubs.acs.org.

References and Notes

(1) Herbst, W.; Hunger, K. *Industrial Organic Pigments: Production, Properties, Applications*; Wiley-VCH: Weinheim, 2004.

(2) Ranke, P.; Bleyl, I.; Simmerer, J.; Haarer, D.; Bacher, A.; Schmidt, H. *Appl. Phys. Lett.* **1997**, *71*, 1332.

(3) Würthner, F.; Thalacker, C.; Diele, S.; Tschierske, C. *Chem.—Eur. J.* **2001**, *7*, 2245.

(4) Jones, B.; Ahrens, M.; Yoon, M.-H.; Facchetti, A.; Marks, T.; Wasielewski, M. *Angew. Chem., Int. Ed.* **2004**, *43*, 6363.

(5) Schmidt-Mende, L.; Fechtenkötter, A.; Müllen, K.; Moons, E.; Friend, R.; MacKenzie, J. *Science* **2001**, *293*, 1119.

(6) Würthner, F.; Chen, Z.; Hoeben, F.; Osswald, P.; You, C.-C.; Jonkheijm, P.; Herrikhuyzen, J.; Schenning, A.; van der Schoot, P.; Meijer, E.; Beckers, E.; Meskers, S. C.; Janssen, R. *J. Am. Chem. Soc.* **2004**, *126*, 10611.

(7) Löhmannsröben, H.-G.; Langhals, H. *Appl. Phys. B* **1989**, *48*, 449.

(8) Kircher, T.; Löhmannsröben, H.-G. *Phys. Chem. Chem. Phys.* **1999**, *1*, 3987.

(9) Würthner, F. *Chem. Commun.* **2004**, 1564.

(10) Grimsdale, A.; Müllen, K. *Angew. Chem., Int. Ed.* **2005**, *44*, 5592.

(11) Hofkens, J.; Latterini, L.; De Belder, G.; Gensch, T.; Maus, M.; Vosch, T.; Karni, Y.; Schweitzer, G.; De Schryver, F.; Hermann, A.; Müllen, K. *Chem. Phys. Lett.* **1999**, *304*, 1.

(12) Rybtchinski, B.; Sinks, L.; Wasielewski, M. *J. Am. Chem. Soc.* **2004**, *126*, 12268.

(13) De Belder, G.; Schweitzer, G.; Jordens, S.; Lor, M.; Mitra, S.; Hofkens, J.; De Feyter, S.; Van der Auweraer, M.; Herrmann, A.; Weil, T.; Müllen, K.; De Schryver, F. *ChemPhysChem* **2001**, *2*, 49.

(14) Mais, S.; Tittel, J.; Basché, T.; Bräuchle, C.; Göhde, W.; Fuchs, H.; Müller, G.; Müllen, K. *J. Phys. Chem. A* **1997**, *101*, 8435.

(15) Lang, E.; Würthner, F.; Köhler, J. *ChemPhysChem* **2005**, *6*, 935.

(16) Lang, E.; Hildner, R.; Engelke, H.; Osswald, P.; Würthner, F.; Köhler, J. *ChemPhysChem* **2007**, *8*, 1487.

(17) Stracke, F.; Blum, C.; Becker, S.; Müllen, K.; Meixner, A. *Chem. Phys. Lett.* **2000**, *325*, 196.

(18) Blum, C.; Stracke, F.; Becker, S.; Müllen, K.; Meixner, A. *J. Phys. Chem. A* **2001**, *105*, 6983.

(19) Stracke, F.; Blum, C.; Becker, S.; Müllen, K.; Meixner, A. *Chem. Phys.* **2004**, *300*, 153.

(20) Stracke, F.; Blum, C.; Becker, S.; Müllen, K.; Meixner, A. *ChemPhysChem* **2005**, *6*, 1242.

(21) Christ, T.; Kulzer, F.; Weil, T.; Müllen, K.; Basché, T. *Chem. Phys. Lett.* **2003**, *372*, 878.

(22) Métivier, R.; Christ, T.; Kulzer, F.; Weil, T.; Müllen, K.; Basché, T. *J. Lumin.* **2004**, *110*, 217.

(23) Fückel, B.; Hinze, G.; Diezemann, G.; Nolde, F.; Müllen, K.; Gauss, J.; Basché, T. *J. Chem. Phys.* **2006**, *125*, 144903.

(24) Izquierdo, M.; Bell, T.; Habuchi, S.; Fron, E.; Pilot, R.; Vosch, T.; De Feyter, S.; Verhoeven, J.; Jacob, J.; Müllen, K.; Hofkens, J.; De Schryver, F. *Chem. Phys. Lett.* **2005**, *401*, 503.

(25) Hofkens, J.; Vosch, T.; Maus, M.; Köhn, F.; Cotlet, M.; Weil, T.; Herrmann, A.; Müllen, K.; De Schryver, F. *Chem. Phys. Lett.* **2001**, *333*, 255.

(26) Hernando, J.; Hoogenboom, J. P.; van Dijk, E. M.; Garcia-Lopez, J. J.; Crego-Calama, M.; Reinhoudt, D. N.; van Hulst, N. F.; Garcia-Parajo, M. F. *Phys. Rev. Lett.* **2004**, *93*, 236404.

(27) Kiraz, A.; Ehrl, M.; Bräuchle, C.; Zumbusch, A. *J. Chem. Phys.* **2004**, *118*, 0010824.

(28) Rebane, K. *Impurity Spectra of Solids*; Plenum Press: New York, London, 1970.

(29) Friedrich, J.; Haarer, D. *Angew. Chem., Int. Ed.* **1984**, *23*, 113.

(30) Maus, M.; Mitra, S.; Lor, M.; Hofkens, J.; Weil, T.; Herrmann, A.; Müllen, K.; De Schryver, F. *J. Phys. Chem. A* **2001**, *105*, 3961.

(31) Vosch, T.; Cotlet, M.; Hofkens, J.; Van Der Biest, K.; Lor, M.; Weston, K.; Tinnefeld, P.; Sauer, M.; Latterini, L.; Müllen, K.; De Schryver, F. *J. Phys. Chem. A* **2003**, *107*, 6920.

(32) Hinze, G.; Haase, M.; Nolde, F.; Müllen, K.; Basché, T. *J. Phys. Chem. A* **2005**, *109*, 6725.

(33) Métivier, R.; Nolde, F.; Müllen, K.; Basché, T. *Phys. Rev. Lett.* **2007**, *98*, 047802.

(34) Fückel, B.; Köhn, A.; Harding, M.; Diezemann, G.; Hinze, G.; Basché, T.; Gauss, J. *J. Chem. Phys.* **2008**, *128*, 074505.

(35) Hinze, G.; Métivier, R.; Nolde, F.; Müllen, K.; Basché, T. *J. Chem. Phys.* **2008**, *128*, 124516.

(36) Engel, E.; Schmidt, K.; Beljonne, D.; Bredas, J.-L.; Assa, J.; Frob, H.; Leo, K.; Hoffmann, M. *Phys. Rev. B* **2006**, *73*, 245216.

(37) Clark, A.; Qin, C.; Li, A. *J. Am. Chem. Soc.* **2007**, *129*, 7586.

(38) Velardez, G.; Lemke, H.; Breiby, D.; Nielsen, M.; Moller, K.; Henriksen, N. *J. Phys. Chem. A* **2008**, *112*, 8179.

(39) Liang, B.; Zhang, Y.; Wang, Y.; Xu, W.; Li, X. *J. Mol. Struct.* **2009**, *917*, 133.

(40) Beljonne, D.; Pourtois, G.; Silva, C.; Hennebiqc, E.; Herz, L. M.; Friend, R. H.; Scholes, G. D.; Setayesh, S.; Müllen, K.; Brédas, J. L. *Proc. Natl. Acad. Sci. U.S.A.* **2002**, *99*, 10982.

(41) Sun, M. *Chem. Phys. Lett.* **2005**, *408*, 128–133.

(42) Renge, I. *J. Opt. Soc. Am. B* **1992**, *9*, 719.

(43) Becke, A. *J. Chem. Phys.* **1993**, *98*, 5648.

(44) Schäfer, A.; Huber, C.; Ahlrichs, R. *J. Chem. Phys.* **1992**, *97*, 2571.

(45) TURBOMOLE v.5.9, http://www.turbomole.com, 2007.

(46) Deglmann, P.; Furche, F.; Ahlrichs, R. *Chem. Phys. Lett.* **2002**, *362*, 511.

(47) Schäfer, A.; Huber, C.; Ahlrichs, R. *J. Chem. Phys.* **1993**, *100*, 5829.

(48) Schirmer, J. *Phys. Rev. A* **1981**, *26*, 2395.

(49) Trofimov, A.; Schirmer, J. *J. Phys. B* **1995**, *28*, 2299.

(50) Hättig, C. *Adv. Quantum Chem.* **2005**, *50*, 37.

(51) Berger, R.; Fischer, C.; Klessinger, M. *J. Phys. Chem. A* **1998**, *102*, 7151.

(52) Jankowiak, H.-C.; Stuber, J.; Berger, R. *J. Chem. Phys.* **2007**, *127*, 234101.

(53) Gierschner, J.; Cornil, J.; Egelhaaf, H.-J. *Adv. Mater.* **2007**, *19*, 173.

(54) Knox, R.; van Amerongen, H. *J. Phys. Chem. B* **2002**, *106*, 5289.

(55) Lippitz, M.; Hübner, C.; Christ, T.; Eichner, H.; Bordat, P.; Herrmann, A.; Müllen, K.; Basché, T. *Phys. Rev. Lett.* **2004**, *92*, 103001.

(56) Basché, T.; Moerner, W.; Orrit, M.; Wild, U. *Single-Molecule Optical Detection, Imaging and Spectroscopy*; VCH: Weinheim, Germany, 1997.

(57) Moerner, W. *Persistent Spectral Hole-Burning: Science and Applications*; Springer: Berlin, 1988.

(58) Press, W. *Single particle rotations in molecular solids*; Springer: Berlin, 1981.

(59) Orrit, M.; Bernard, J.; Zumbusch, A.; Personov, R. I. *Chem. Phys. Lett.* **1992**, *196*, 595.

(60) Hennebicq, E.; Beljonne, D.; Curutchet, C.; Scholes, G. D.; Silbey, R. J. *J. Chem. Phys.* **2009**, *130*, 214505.

JP909862X